

Thickness of Crust in the West of Iran Obtained from Modeling of Ps Converted Waves

Khatami, M. S.¹, Taghizadeh-Farahmand, F.^{2*} and Afsari, N.³

1. M.Sc. Student, Department of Physics, Qom Branch, Islamic Azad University, Qom, Iran

2. Associate Professor, Department of Physics, Qom Branch, Islamic Azad University, Qom, Iran

3. Assistant Professor, Department of Civil Engineering, Nowshahr Branch, Islamic Azad University, Nowshahr, Iran

(Received: 14 Jan 2018, Accepted: 25 Sep 2018)

Abstract

Receiver functions are usually used to detect Ps converted waves and are especially useful to picture seismic discontinuities in the crust and upper mantle. In this study, the P receiver function technique beneath the west Iran is used to map out the lateral variation of the Moho boundary. The teleseismic data ($M_b \geq 5.5$, epicentral distance between 30° - 95°) recorded from 2004 to 2016 at 17 permanent broadband and short-period stations of the Iranian Seismological Center (ISC, <http://irsc.ut.ac.ir>) of Kermanshah, Khoramabad, Hamedan and Boroujerd and one broadband station of the International Institute of Earthquake Engineering and Seismology (IIIES, <http://www.iiies.ac.ir>) were used. The results indicate clear Ps conversions at the Moho boundary. The Moho depths are estimated from the delay time of the Moho converted phase relative to the direct P wave beneath each network. The average Moho depth lies at $\sim 42 \pm 2$ km. Furthermore, the clear image of the Moho at depths as modeling of PRF, ranging from 37 km beneath KCHF station to maximum 55 km beneath HAGD station was presented. According to the distribution and number of stations used, this study is more comprehensive than previous studies.

Keywords: P Receiver Function, Crustal Structure, Converted Waves, Northwest of Zagros, Iran.

1. Introduction

The Zagros fold-thrust belt extends 2000 km from Turkey in the NW to the Hormuz Strait in the SE (James and Wynd, 1965) resulted from the collision of Arabian Plate with the continental crust of Central Iran after the closure of the Neotethys Ocean (Dewey and Grantz, 1973). The Zagros collision zone comprises of three major sub-parallel tectonic elements. They are, from SW to NE, the Zagros Fold and Thrust Belt (ZFTB), the Sanandaj-Sirjan Metamorphic Zone (SSZ), and the Urmieh-Dokhtar Magmatic Arc (UDMA) (Stöcklin, 1968; Ricou et al., 1977). There are some main active faults in the west of Iran. ZFTB is bounded to the north by the Main Zagros Reverse Fault (MZRF), (Stöcklin, 1974), which have been considered to be the active thrust fault between Arabia and Iran during subduction and before suturing occurred (i.e. Falcon, 1974). High Zagros Fault (HZF) is another major fault in the ZFTB in the NW-SE trending (Falcon, 1974; Berberian, 1995), which marks the High Zagros with the highest topography in the region (Fig. 1). Earthquake data show that most of the activity is concentrated along the Zagros fold-thrust belt in Iran. The region referred as northwest of Zagros of Iran in this study includes the area located between 46° - 50° longitude and 33° - 36° latitude (Fig. 1).

The Moho discontinuity has been extensively studied with different methods and data in Zagros region (Asudeh, 1982; Dehghani and Makris, 1984; Snyder and Barazangi, 1986; Hatzfeld et al., 2003). Recently, Paul et al. (2006, 2010) showed the migrated sections computed from P receiver functions (PRF) and their results revealed an average crustal thickness of 42 ± 2 km beneath the Zagros Fold and Thrust Belt implying that the crystalline crust of ZFTB has not been significantly thickened by the collision yet. They showed a crustal model with a maximum crustal thickness of ~ 70 km underneath SSZ. Even though, they found a thick crust beneath the UDMA ~ 50 km along the Northwest Zagros profile. They also explained the thickening by overthrusting of the Arabia margin crust by the crust of central Iran along the Main Zagros Recent Faults (MZRF). Shad Manaman and Shomali (2010) and Shad Manaman et al. (2011) propose a maximum 65 km depth for the Zagros region on the same profile as Paul et al. (2006), but their maximum crustal thickness is some 50 km further SW. A more recent study by Afsari et al. (2011), based on receiver functions modeling, indicates an average Moho depth of about 42 km beneath the Northwest Zagros increasing toward the

*Corresponding author:

f_farahmand@qom-iau.ac.ir

SSZ and reaches 51 km and the Moho depth decreases toward the UDMA belt and reaches 43 km beneath this area. Recently, Motaghi et al. (2017) via S-wave velocity model showed that the crustal thickness beneath Zagros increases from 43 to 59 km beneath main recent fault and crustal thickness reaches maximum depth of 62 km beneath SSZ. Karimizadeh et al. (2017) deduced the average of Moho depth based on PRF and Zhu and Kanamori (2000) method via data from 10 short period and broadband stations ~44 km beneath Northwest of Zagros (Kermanshah and Khoramabad).

This study intends to improve the knowledge of crustal structure beneath the Northwest Zagros. The main goal of this paper is to resolve the map of Moho depth beneath the west of Iran (Northwest of Zagros) using data from 15 broadband and 3 short-period permanent seismological stations located in this region from PRF modeling. This is the first modeling study on teleseismic data recorded by Hamedan, Boroujerd, and Khoramabad Seismic Networks.

2. Data and Methodology

The data used for this study were recorded by the Iranian Seismological Center (ISC), which consists of four Seismic Networks, Kermanshah, Khoramabad, Hamedan, and

Boroujerd with 17 permanent broadbands (CMG3ESP-120s, CMG3T-360s, Trillium-240s) and short period (SS1, 1-Hz) seismic stations. In addition, the data from one broadband (Güralp-120s) stations (SNGE) operated by the International Institute of Earthquake Engineering and Seismology (IIEES) was used (Fig. 1). Names and coordinates of the stations are listed in Table 1.

More than 1000 teleseismic events (Fig. 2) with magnitudes greater than 5.5 (Mb) at epicentral distances between 30° - 95° in a time period between 2004 and 2016 for P receiver function analysis were used. Data were recorded by ISC and IIEES.

The methodology used in this study is to calculate P receiver functions in each station the same as Yuan et al. (1997). The three components ZNE are rotated into the local ray coordinate system LQT using theoretical back azimuth and incidence angle. To isolate the P-to-S conversions on the Q component, the L component is deconvolved from the Q component. Finally, a distance correction (moveout correction) was applied prior to stacking using a reference epicentral distance of 67° (corresponding to ray parameter of 6.4 s°) according to the IASP91 reference velocity model (Kennett and Engdahl, 1991).

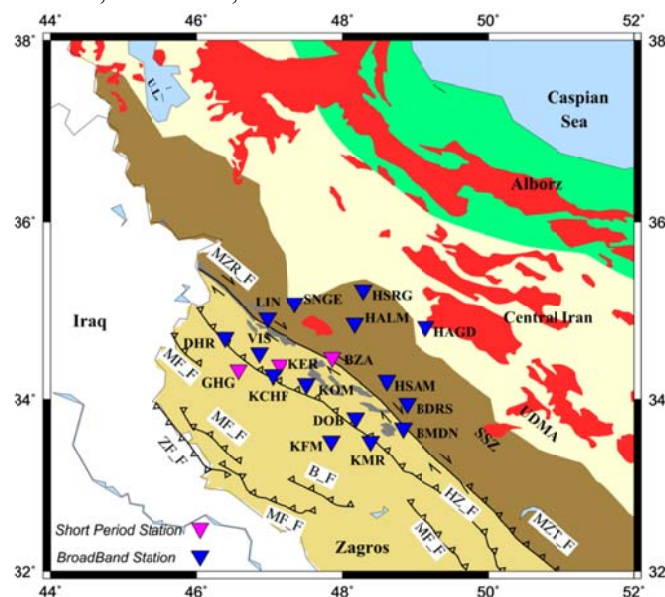


Figure 1. Location map of the seismological stations used in this study. The main faults are shown by the black lines (Faults from Hessami et al., 2003). Blue and pink triangles show broadband and short period seismological stations, respectively. Red spots show volcanic and intrusive rocks. MZT_F (Main Zagros Thrust Fault), SSZ (Sanandaj-Sirjan Zone), UDMA (Urumieh-Dokhtar Magmatic Arc), MZR_F (Main Zagros Thrust Fault), MF_F (Mountain Front Fault), HZ_F (High Zagros Fault, B_F (Balarud Fault) and ZF_F (Zagros Foredeep Fault).

Another step often employed in receiver function analysis is inversion of the time domain waveforms to find the most suitable crustal thickness and velocity beneath each seismic station. There is no guarantee that a unique inversion result will be obtained, as the method seeks to minimize the differences between observed and synthetic receiver functions. The method may be successful for different pairs of starting and final models, indicating that the final model depends on the choice of a physically reasonable starting model. Undesirable results occur if no clear converted phases or multiples exist in the time domain receiver functions, because in such cases, seismic noise may be transformed into a velocity-depth model. Therefore, forward modeling of the receiver functions as described by Kumar et al. (2007) is preferred. The first step is to identify the Moho conversion in the waveform, which is often the biggest phase on the Q component. Other phases frequently detected in time domain receiver functions are conversions from the bottom of a sedimentary layer and crustal multiples. The arrival times of all these phases were selected and by forward modeling a crustal model was found that fits the waveforms reasonably well; however, the main aim is to estimate the Moho depth. For

starting PRF modeling, Q and L components were summed for each station in the time window from -5 s prior to the zero phase P wave to 30 s after it. To achieve stability in the forward modeling, both crustal conversions and their strongest multiples and sedimentary conversions are modeled.

3. P receiver function observations

Teleseismic events with a relatively high signal-to-noise ratio (>4) have been carefully selected at each station. A time window of 110 s, starting 10 s before the P-onset arrival time was considered. In the first step, to isolate the receiver effects of the seismograms recorded at different instruments, the respective instrument responses has to be deconvolved from the seismographs. ZNE components are then rotated into the local LQT ray-based coordinate system. To isolate the P-to-S conversions on the Q component, the L component is deconvolved from the Q component. A low-pass filter of 2 s is applied to the PRF. They are stacked after move-out correction for a reference slowness of 6.4 s $^\circ$, according to the IASP91 velocity model (Kennett et al., 1991). Figure 3 shows the processing steps for a data at the HALM station.

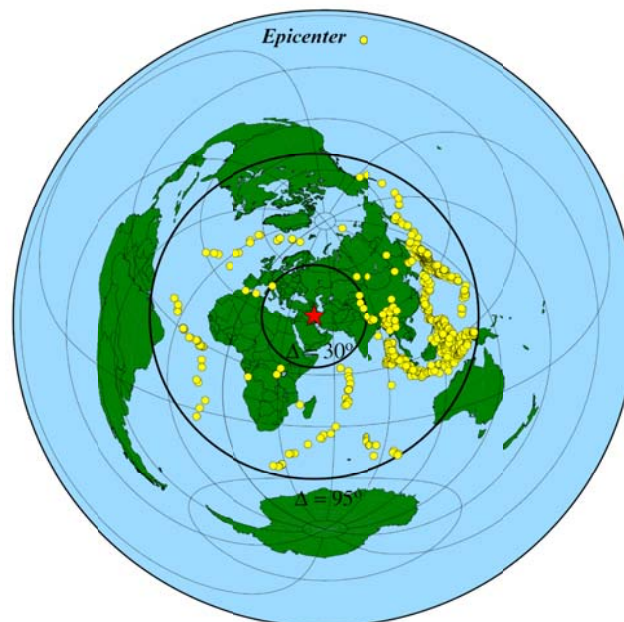
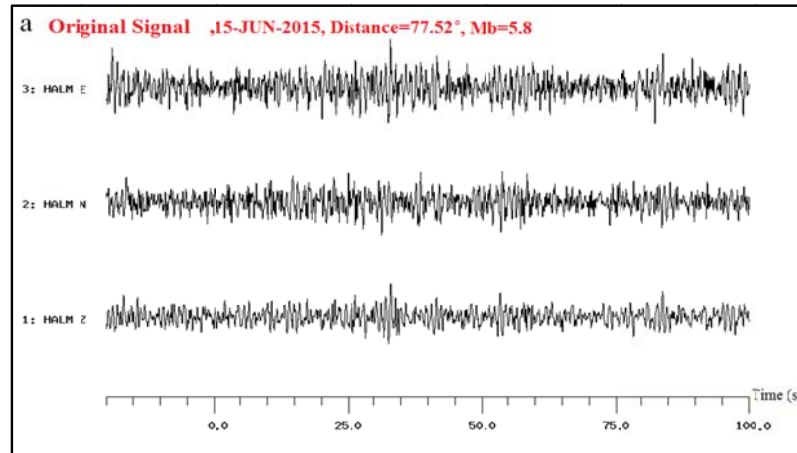


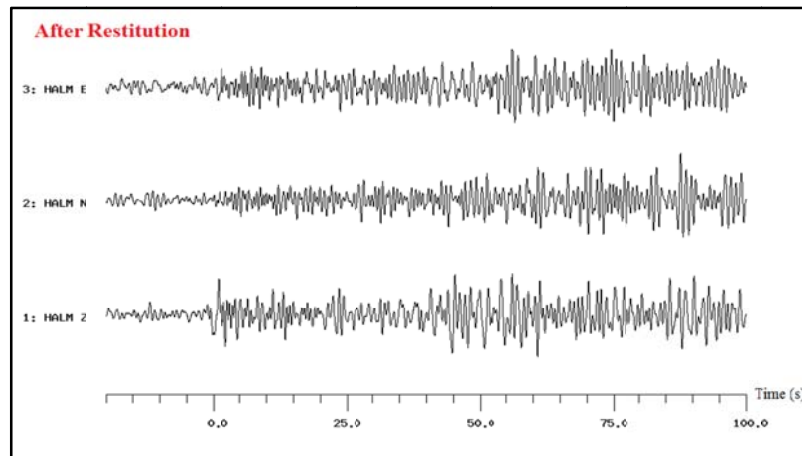
Figure 2. Distribution of teleseismic events recorded by different seismological networks used in this study (ISC and IIEES) between 2004 and 2016 and used to calculate P receiver functions. The red star represents the approximate position of the area of this study. The black solid circles mark the 30° and 95° epicentral distances, respectively.

Figure 4 shows the value of delay time of converted phase in study area beneath each station. The minimum delay time of the Moho converted phase (4.5 s) is observed beneath the station LIN located in the

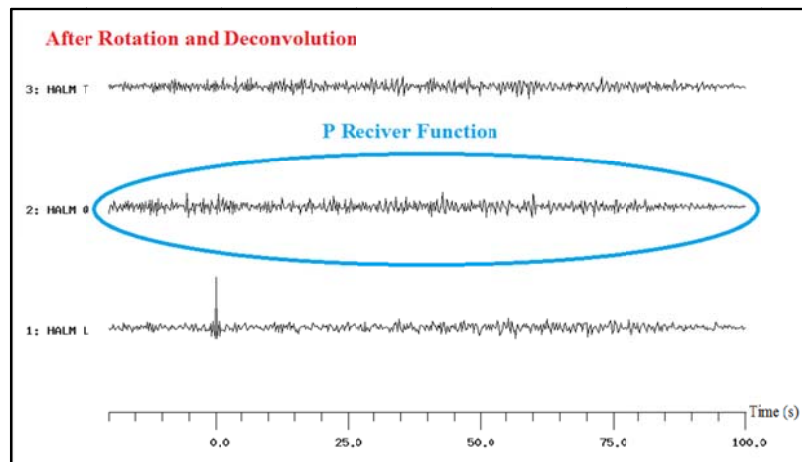
western part of an area in this study. Even though, the largest delay time (6.5 s) is seen beneath the stations KMR and HAGD located in the southern and northern parts of the study area, respectively.



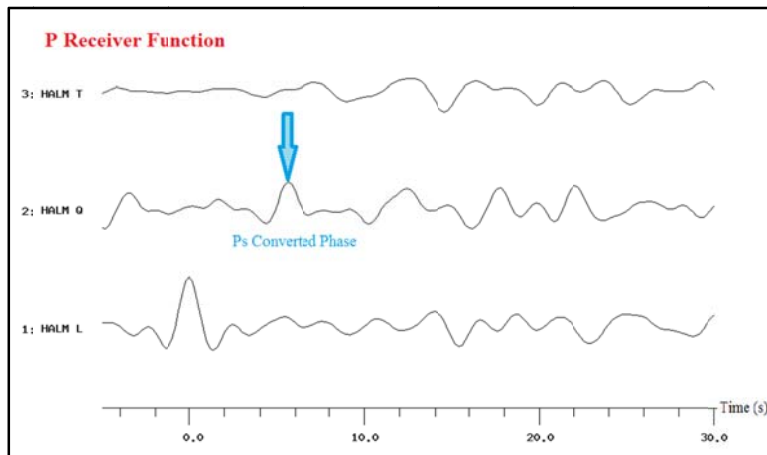
(a)



(b)



(c)



(d)

Figure 3. A data example to show the PRF steps. a) An original recording of the earthquake on June 15, 2015 recorded at stations: broadband (HALM). b) The components after restitution of the instrument response. The P onset is assumed to be as zero time. c) The components after rotation into LQT ray-based system under the theoretical back azimuth and incidence angle and P waveform are deconvolved from all three components. d) The components are in the time window of -5-30 s. The first converted Ps phase at ~5s represents the conversion from the Moho that is shown with the blue narrow.

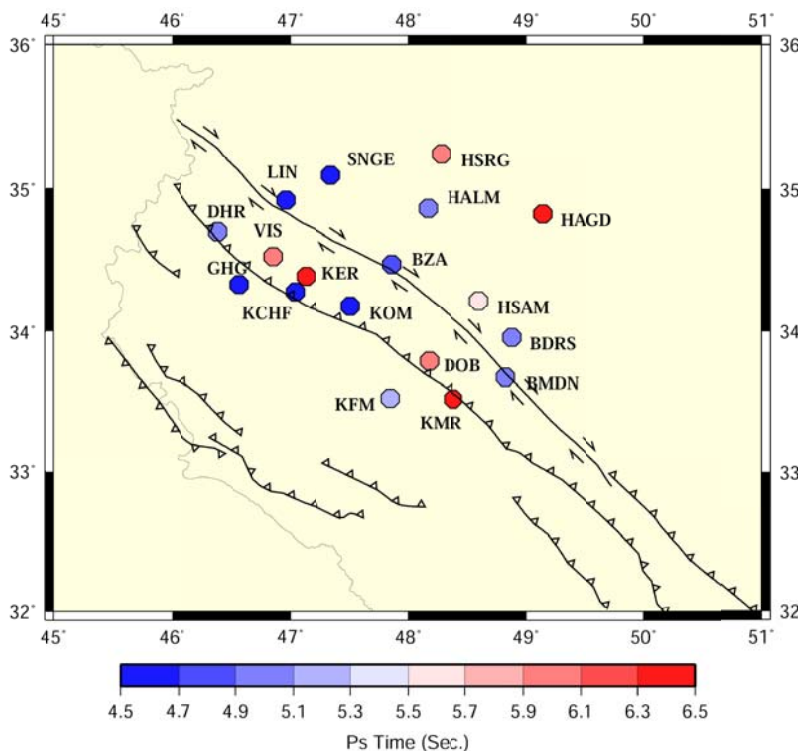


Figure 4. Ps delay time of the Moho converted phase beneath each station in West of Iran.

Individual and stacked PRFs for some stations are presented in Figure 5. PRFs are sorted by increasing back azimuth. The most coherent conversion is, however, the

conversion at the Moho boundary (marked Moho Ps) arriving between 4.6 and 6.4 s delay time in Figure 5.

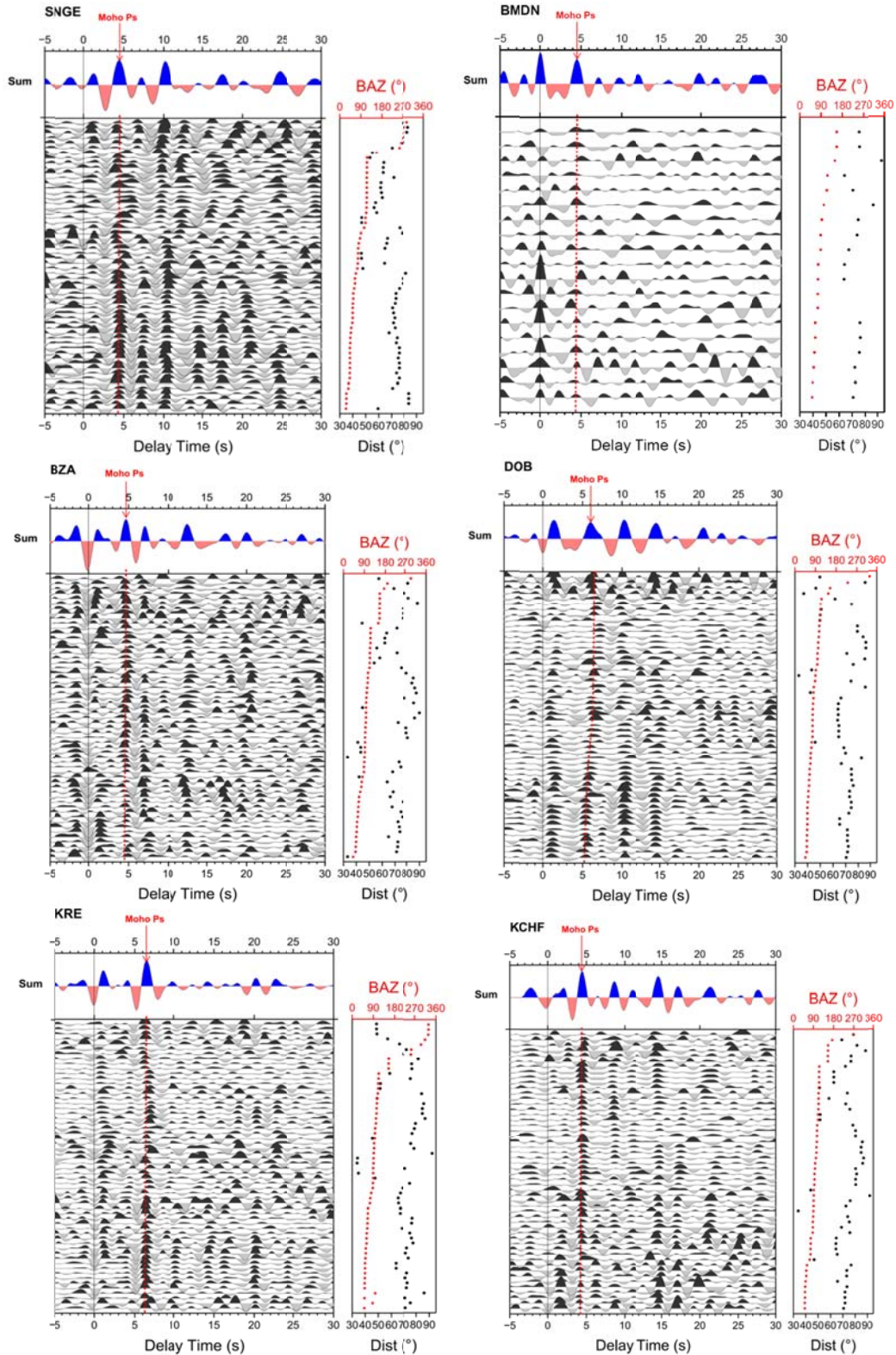


Figure 5. Individual PRFs with summation traces for some stations. Individual seismograms are plotted equally spaced and sorted by increasing back azimuth (red rectangles). Black dots indicate the epicentral distances (shown in the right). They are filtered with a low-pass filter of 2s. The P onset is fixed at zero time. The Ps conversion phases from the Moho are labeled on the summation traces (marked Moho Ps).

4. Crustal thickness

An initial estimation of the Moho depth can be obtained from the delay time of the corresponding Ps conversion by using available velocity model obtained from the previous geophysical studies in the west of Iran (Paul et al., 2010, Afsari et al., 2011).

The Moho depths are listed in Table 1 (marked by Moho depth as the previous study). The Moho depth varies between 36.5 km in LIN station and 52 km in KMR and HAGD stations. Figure 6 presents contours of Moho depth at each station by the procedure of Ps time.

In the second step, the forward modeling of the P receiver functions was utilized to find the most suitable crustal thickness beneath each station. For this aim, the first step is to identify the Moho conversion, which can be easily performed due to the clear appearance of the Moho phase in the data. P wave velocity models are used as previous study

(Paul et al., 2010; Afsari et al., 2011) for the first model.

In the previous section, the thickness of the crust was calculated using the velocity model of previous studies in the study area. Different thicknesses of Moho and P wave velocity models were modeled from previous section. By changing the depth of Moho and the V_p/V_s ratio, respectively, the overlapping time of the Moho phases and their strongest multiples in the theoretical and observational model were improved. The optimal parameters of the model are found by iteratively minimizing the root mean square difference between the observed and theoretical traces. Only the resulting models for which the root mean square decreased significantly were kept. After modeling, the models with a small root mean square error less than 0.025 were selected. Figure 7 illustrates the results of forward modeling for station SNGE.

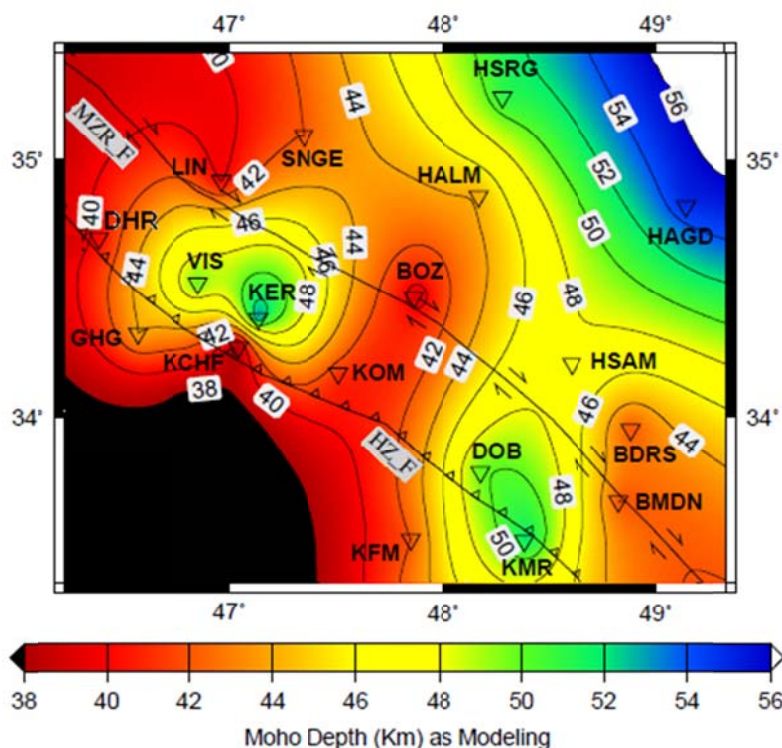


Figure 6. The contour map of Moho depth beneath each station in West of Iran.

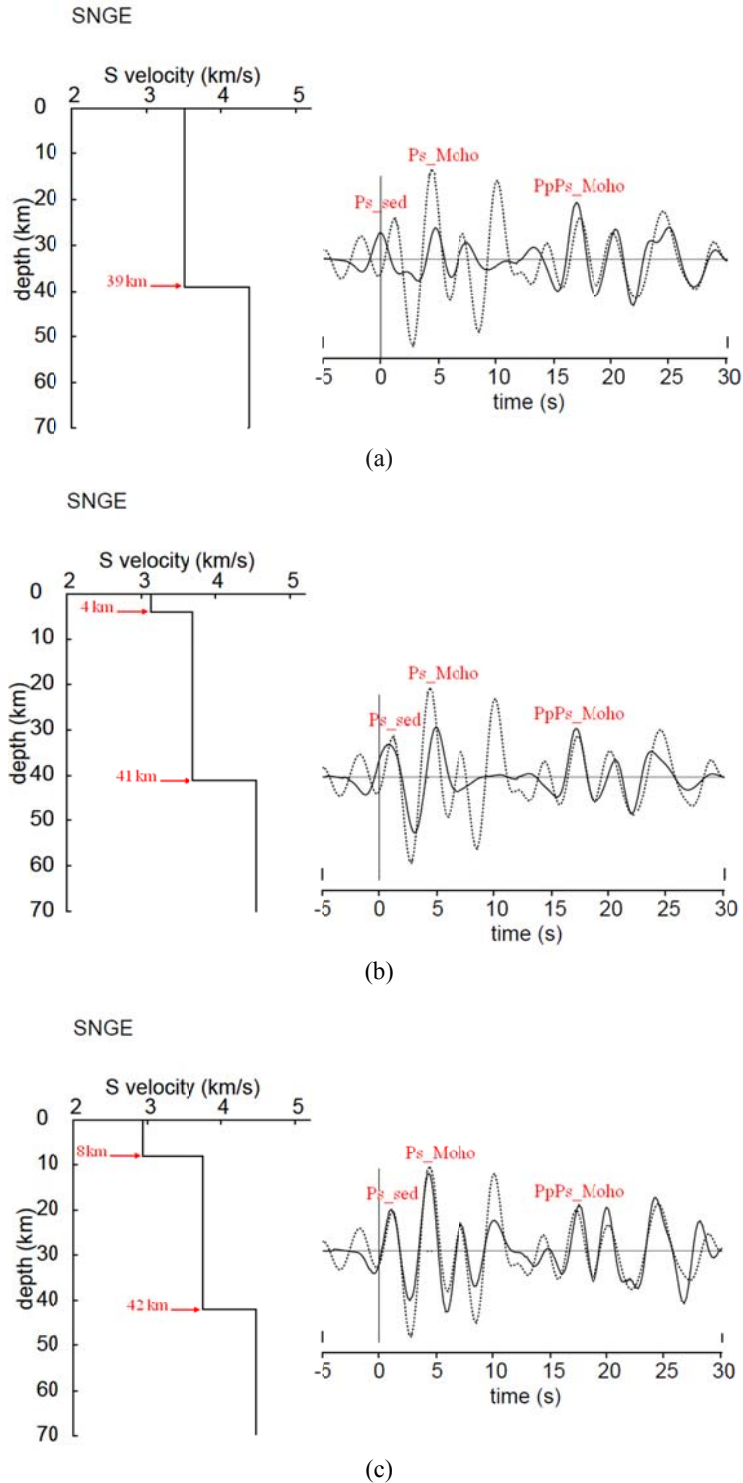


Figure 7. Forward modeling of the stacked traces in SNGE station. The dashed line in the right panel of each part is the observed receiver function, and the solid lines are the synthetic receiver functions corresponding to the different models. a) Considering a layer for the crust, model fits the primary Ps conversion of Moho and crustal multiples (PpPs) point of view their delay times. b) Considering two layers for the crust, model containing an additional thick layer at the surface, fits the first conversion near 1 s and as well the Moho conversion (Ps), and their strongest multiples (marked as PpPs) and conversions from the bottom of a sedimentary layer (marked as Ps-sed) are considered and waveform has good coverage.

Figure 7 shows three models among many models that are selected to find the best crustal model to obtain a depth of Moho. Best models are those that their Moho phases and strongest multiples have acceptable coverage point of view for their delay times, amplitudes and waveforms. Right panel of the Figure 7 represent a comparison between computed and observed traces for some models shown in the left parts. The solid lines indicate the theoretical receiver functions, and the dashed lines indicate the observed receiver functions. Model 7-a fits the primary Ps conversion of Moho and crustal multiples (PpPs) point of view their delay times. Model 7-b, containing an additional 4 km thick layer at the surface, fits the first conversion near 1 s as well as the Moho conversion (Ps). It causes Moho

phases and their strongest multiples to have acceptable coverage point of view for their amplitudes. Both pairs of depths and velocity model were changed to find optimum model with small root mean square error less than 0.025. Figure 7-c shows the best model for this station SNGE, the Moho phases (marked as Ps), and their strongest multiples (marked as PpPs) and conversions from the bottom of a sedimentary layer (marked as Ps-sed) are considered. The arrival times of all these phases (Moho conversion phase and crustal multiples) were picked and by forward modeling, a crustal model was found that fits the waveforms reasonably well. The best model is shown for some stations in Figure 8. Moho conversion times, as well as the Moho depths, are listed in Table 1 (marked by Moho depth as modeling).

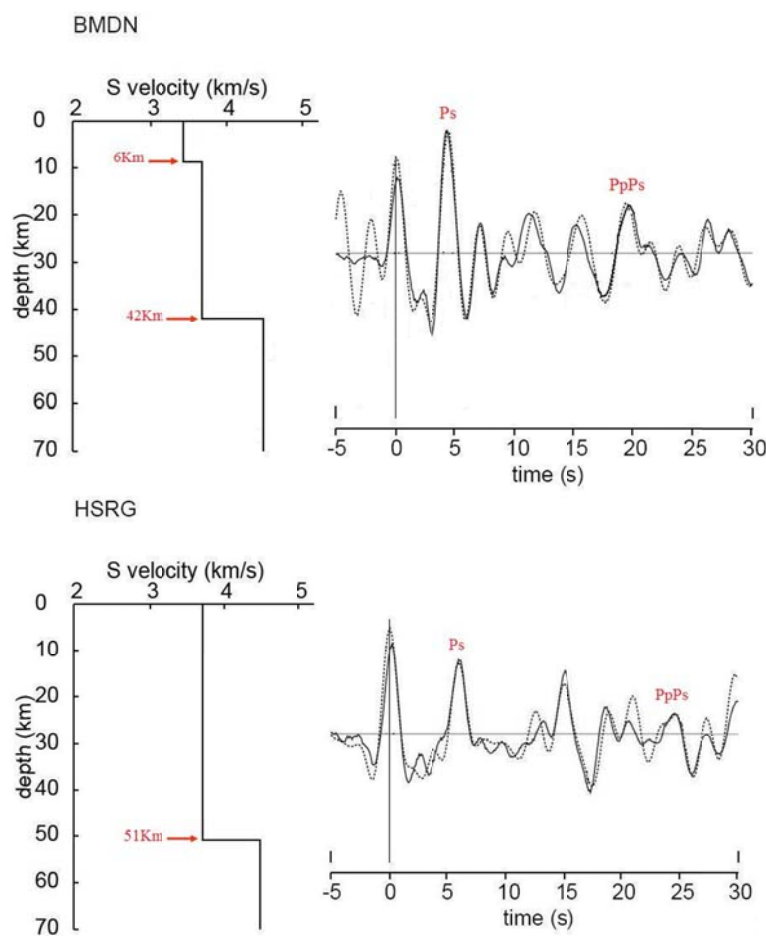


Figure 8. Best forward modeling of the stacked traces in BMDN and HSRG stations. The Moho phases (marked as Ps), and their strongest multiples (marked as PpPs) are considered and waveform has good coverage.

5. Result and Interpretation

The crustal thickness using P receiver function modelings beneath the broadband and short period stations in the west of Iran was determined. Figure 9 shows the contour of Moho depth beneath the stations, which exactly deduced from P receiver function modeling. The Moho depth map significantly presents a crustal thickening from southwest towards the northeast. This may be related to the collision between the Arabian and Central Iran plates and could show the crustal shortening occurring in the west of Iran. The present-day convergence between Arabia and Eurasia is 19-23 mm/yr along the Zagros folded belt (McClusky et al., 2003), and there is 4 ± 2 mm.yr⁻¹ shortening in the west of Iran according to Vernant et al. (2004). The results of PRF show that the average Moho depth in the northwest of Zagros (Kermanshah, Khoramabad, Hamedan and Boroujerd region) is about $\sim 43 \pm 2.5$ km, which is in good agreement with the results obtained by PRF modeling ($\sim 47 \pm 2.5$).

Besides, the results show two local thickening beneath KER and KMR (53 and 52 km, respectively) stations, which are in

good agreement by Afsari et al. (2011) and Karimizadeh et al. (2017). Probably this crustal thickening below these stations is related to the overthrusting system in this area, previously described by Berberian (1995).

The result correlates also well with that obtained by Jimenez-Munt et al. (2012) by residual Bouguer anomalies. A more recent study by Taghizadeh-Farahmand et al. (2015), based on receiver functions modeling, obtained the thickness of the Moho that is varied between 42 and 48 km via data from six short period stations in this region. The results are in good agreement with those obtained from other studies (Paul et al., 2006, 2010; Hatzfeld et al., 2003). Paul et al. (2006) proposed that the crust of Central Iran overthrusts the crust of Zagros on the MZRF interpreted as a crustal-scale structure rooted at Moho depth.

Due to the proper distribution of stations and also a significant increase in the number of stations, the results obtained in this study are more complete and accurate than previous studies, especially the receiver function modeling method.

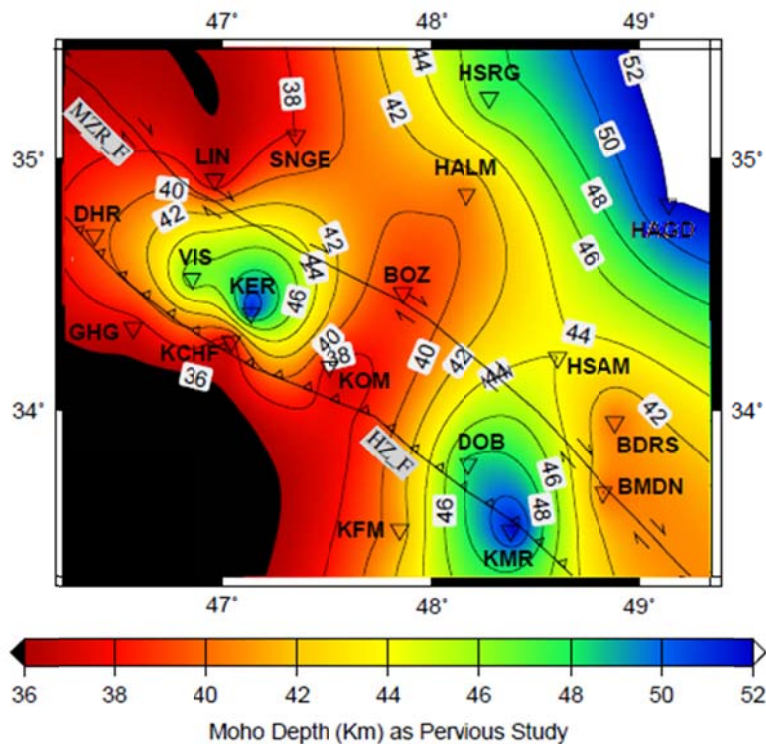


Figure 9. The contour map of Moho depth beneath each station in West of Iran as PRF modeling.

Table1. Specification of the seismic stations, Ps conversion times (Sec.), corresponding depths (km).

Network	Code Station	Arrival Time of Ps Phase (Sec.)	Moho Depth (± 2.5 km) as (Paul et al., 2010, Afsari et al., 2011)	Moho Depth (± 2.5 km) as Modeling	Lat.N (Deg.)	Long.E (Deg.)	Elevation (m)
Kermanshah	DHR	4.9	39.5	40.0	34.700	46.387	1840
	KOM	4.6	37.0	41.0	34.176	47.514	1716
	GHG	4.6	37.0	44.0	34.329	46.568	2060
	LIN	4.5	36.5	40.0	34.919	46.963	2140
	VIS	5.9	47.5	50.0	34.528	46.851	1833
	BZA	4.7	38.0	39.0	34.470	47.861	2330
	KCHF	4.6	37.0	38.0	34.275	47.040	1715
	KER	6.4	51.5	53.0	34.387	47.133	1338
Khoramabad	DOB	6.0	48.5	50.0	33.787	48.177	1948
	KFM	5.1	41.0	42.0	33.524	47.847	1676
	KMR	6.5	52.0	52.0	33.518	48.38	1733
Hamedan	HAGD	6.5	52.0	55.0	34.822	49.139	1831
	HALM	5.0	40.0	44.0	34.860	48.168	2450
	HSAM	5.5	44.0	48.0	34.212	48.602	2314
	HSRG	5.9	47.5	51.0	35.242	48.279	2545
Boroujerd	BDRS	5.0	40.0	42.0	33.954	48.881	2494
	BMDN	5.0	40.0	42.0	33.672	48.825	1698
INSN	SNGE	4.7	38.0	42.0	35.093	47.347	1940

6. Conclusion

The Moho discontinuity beneath west of Iran is resolved using 17 permanent broadband and short-period stations of the Tabriz Telemetry Seismic Network of Kermanshah, Khoramabad, Hamedan and Boroujerd and one broadband station of SNGE by using P receiver function modeling. The average Moho depth in the west parts of Iran is about $\sim 47 \pm 2.5$ km and Moho discontinuity is not flat. We have been able to present a clear image of the Moho at depths ranging from 38 km beneath KCHF station to Maximum 55 km beneath HAGD station in the southern and northern part of the study area, respectively. The Moho depth map significantly presents a crustal thickening from the southeast towards the northeast.

Acknowledgements

Authors are grateful to the Iranian Seismological Center (ISC, <http://irsc.ut.ac.ir>) and the International Institute of Earthquake Engineering and Seismology (IIEES, <http://www.iiees.ac.ir>) for providing the teleseismic waveforms. The software packages of Seismic Handler (Stammler, 1993) were used for data processing and GMT (Wessel and Smith, 1998) was used for plotting.

References

- Afsari, N., Sodoudi, F., Taghizadeh-Farahmand, F. and Ghassemi, M.R., 2011, Crustal structure of Northwest Zagros (Kermanshah) and Central Iran (Yazd and Isfahan) using teleseismic Ps converted phases. *Journal of Seismology*, 15, 341–353.
- Asudeh, I., 1982, Seismic structure of Iran from surface and body wave data. *Geophys. J. R. Astr.*, 71, 715-730.
- Berberian, M., 1995, Master “blind” thrust faults hidden under the Zagros folds; active basement tectonics and surface morphotectonics. *Tectonophysics*, 241, 193–224.
- Dehgani, G. A. and Makris, J., 1984, The Gravity field and crustal structure of Iran. *N. Jb. Geol. Palaont Abh.*, 168, 215-229.
- Dewey, J. W. and Grantz, A., 1973, The Ghir earthquake of April 10, 1972 in the Zagros mountains of southern Iran; seismotectonic aspects and some results of a field reconnaissance. *Bull. Seismol. Soc. Am.*, 63, 2071–2090.
- Falcon, N. L., 1974, Southern Iran: Zagros Mountains. *Spec. Pub. Geol. Soc. Lond.*, 4, 199–211.
- Hatzfeld, D., Tatar, M., Priestley, K. and Ghafory-Ashtyany, M., 2003, Seismological constraints on the crustal structure beneath the Zagros mountain belt (Iran). *Geophysical Journal International*, 155, 403–410.
- Hessami, KH., Jamali, F. and Tabassi, H., 2003, Major Active Faults of Iran, International Institute of Earthquake Engineering and Seismology, Department of Seismotectonic, Seismology Research Center, Tehran, Iran.
- James, G. A. and Wynd, J. G., 1965, Stratigraphic nomenclature of Iranian Oil Consortium Agreement area. *American Association of Petroleum Geologists Bulletin*, 49, 2182-2245.
- Jimenez-Munt, I., Fernandez, M., Saura, E., Verges, J. and Garcia-Castellanos, D., 2012, 3-D lithospheric structure and regional/residual Bouguer anomalies in the Arabia–Eurasia collision (Iran). *Geophys. J. Int.*, 190, 1311–1324.
- Karimizadeh, S., Afsari, N. and Taghizadeh-Farahmand, F., 2017, Seismic image of the crustal structure in Kermanshah and Khorramabad region, northwest of Zagros, using teleseismic waves. *Journal of Research on Applied Geophysics*, 3(2), 217-227.
- Kennett, B.L.N., Engdahl, E.R. and Buland, R., 1995, Constraints on seismic velocities in the Earth from traveltimes. *Geophys. J. Int.*, 122(1), 108-124.
- Kumar, P., Yuan, X., Kumar, M.R., Kind, R., Li, X. and Chadha, R.K., 2007, The rapid drift of the Indian tectonic plate, *Nature*, 449, 894–897, doi:10.1038/nature06214.
- McClusky, S., Reilinger, R., Mahmoud, S., Ben Sari, D. and Tealeb, A., 2003, GPS constraints on Africa (Nubia) and Arabia plate motion. *Geophys. J. Int.*, 155, 126–138.
- Motaghi, K., Shabanian, E. and Kalvandi, F., 2017, Underplating along the northern portion of the Zagros suture zone, Iran. *Geophysical Journal International*, 210, 375–389. doi: 10.1093/gji/ggx168.
- Paul, A., Kaviani, A., Hatzfeld, D., Vegne, J.

- and Mokhtari, M., 2006, Seismological evidence for crustal-scale thrusting in the Zagros mountain belt (Iran). *Geophys. J. Int.*, 166, 227–237, doi: 10.1111/j.1365-244x.2006.02920.x.
- Paul, A., Hatzfeld, D., Kaviani, A., Tatar, M. and Pequegnat, C., 2010, Seismic imaging of the lithospheric structure of the Zagros mountain belt (Iran). *Geol. Soc. London Special Publications*, 330, 5-18.
- Ricou, L., Braud, J. and Brunn, J.H., 1977, Le Zagros, *Mem. Soc. Geol. Fr.*, 8, 33–52.
- Shad Manaman, N. and Shomali, H., 2010, Upper mantle S-velocity structure and Moho depth variations across Zagros belt, Arabian-Eurasian plate boundary, *Phys. Earth Planet Inter.*, 180, 92–103.
- Shad Manaman, N., Shomali, H. and Koyi, H., 2011, New constraints on upper-mantle S-velocity structure and crustal thickness of the Iranian plateau using partitioned waveform inversion. *Geophys. J. Int.*, 184, 247–267.
- Snyder, D.B. and Barazangi, M., 1986, Deep crustal structure and flexure of the Arabian plate beneath the Zagros collisional mountain belt as inferred from gravity observation. *Tectonics*, 5, 361–373.
- Stammler, K., 1993, Seismic handler programmable multichannel data handler for interactive and automatic processing of seismological analyses, *Comput. Geosci.* 19, 135–140.
- Stöcklin, J., 1968, Structural History and Tectonic of Iran: A Review. American Association of Petroleum Geologists Bulletin, USA, 52, 1229-1258.
- Stöcklin, J., 1974, Possible ancient continental margins in Iran. In C.A. Burk and C.L. Drake (Eds.), *The Geology of Continental Margins*. Springer-Verlag, New York, 873-887.
- Taghizadeh-Farahmand, F., Afsari, N. and Sodoudi, F., 2015, Crustal Thickness of Iran Inferred from Converted Waves. *Pure and Applied Geophysics*, 171, 2, 309-331.
- Vernant, Ph., Nilforoushan, F., Hatzfeld, D., Abbassi, M.R., Vigny, C., Masson, F., Nankali, H., Martinod, J., Ashtiani, A., Bayer, R., Tavakoli, F. and Chery, J., 2004, Present-day crustal deformation and plate kinematics in the Middle East constrained by GPS measurements in Iran and northern Oman. *Geophys. J. Int.*, 157, 381-398.
- Wessel, P. and Smith, W.H.F., 1998, New, improved version of Generic Mapping Tools Released. *EOS Trans. Am. Geophys. Union*, 79, 579.
- Yuan Y., Huang, Q. and Wu, H.M., 1997, Myosin light chain phosphorylation: modulation of basal and agonist-stimulated venular permeability. *American Journal of Physiology*, 272, H1437–1443.
- Zhu, L. and Kanamori, H., 2000, Moho depth variation in southern California from teleseismic from receiver functions. *Journal of Geophysical Research*, 105(82), 2969-2980.